Study of an Isolated Dust Structure near by the White Dwarf WD0011-399 Using IRIS, AKARI, and WISE Data

S. Rijal, S. Sigdel, and M. S. Paudel

Journal of Nepal Physical Society
Volume 8, No 2, 2022
(Special Issue: ANPA Conference 2022)
ISSN: 2392-473X (Print), 2738-9537 (Online)

JNPS, **8** (2), 14-22 (2022)
DOI: http://doi.org/10.3126/jnphyssoc.v8i2.50140

Published by: Nepal Physical Society
P.O. Box: 2934
Tri-Chandra Campus
Kathmandu, Nepal
Email: nps.editor@gmail.com

ANPA Conference 2022
ISSN : 2392-473X(Print), 2738-9537 (Online)

DOI:http://doi.org/10.3126/jnphyssoc.v8i2.50140

Study of an Isolated Dust Structure Nearby the White Dwarf WD0011-399 Using IRIS, AKARI, and WISE Data

S. Rijal,[1, a)] S. Sigdel,[2, b)] and M. S. Paudel[2, c)]

[1)]*Department of Physics, Tri-Chandra Multiple Campus, Tribhuvan University, Nepal*
[2)]*Department of Physics, Tri-Chandra Multiple Campus, Tribhuvan University, Nepal*

[a)]*Corresponding author: sanjay1.745401@trc.tu.edu.np*
[b)]*Electronic mail: sushilasigdel11@gmail.com*
[c)]*Electronic mail: mspaudel27@gmail.com, madhu.paudel@trc.tu.edu.np*

Abstract. During the asymptotic giant branch (AGB) phase, a major fraction of mass is spread by the stars (0.6 - 10 $M_\odot$) in the interstellar medium (ISM) in the form of dust. In the left phase of the post-main sequence evolution in the Hertzsprung-Russell (HR) diagram, these dust are found to be surrounding the white dwarfs (WD). Some small fraction of dust is also formed in the circumstellar shells and cavities around WD which is usually a source of infrared (IR) excess. The formation and evolution of such IR dust structures are the results of high-pressure events such as the Helium shell flash (thermal pulse) and stellar winds, and such structures are crucial in the study of interaction phenomena in ISM. This research project is focused on the study of an isolated dust structure near the white dwarf WD0011-399 located at R.A. (J2000) $00^h\ 13^m\ 47.48^s$ and Dec. (J2000) $-39^\circ\ 37'\ 24.28''$ using Improved Reprocessing of the IRAS (IRIS), AKARI and Wide-field Infrared Survey Explorer (WISE) surveys from SkyView Virtual Observatory along with SIMBAD Astronomical Database and Gaia Archive of ESA. The size of the cavity under study is 7.43 pc$\times$2.90 pc, 2.99pc$\times$0.99pc, and 1.26$\times$0.53pc with an inclination angle of 71.12°, 75.73°, and 68.48° respectively in IRIS, AKARI and WISE data suggesting the cavity is neither a face-on nor an edge-on. The relative flux density of the region has been studied through pixel extraction of Far-Infrared (FIR) images and dust color temperature along with dust mass has been calculated. Using IRIS data, the temperature of the isolated region is found between a maximum value of 36.82$\pm$4.30 K to a minimum of 22.59$\pm$2.32 K with an offset of 14.23 K. The average temperature of the region is 28.22$\pm$0.18 K. Following similar procedures for AKARI data, the temperature is found between a maximum of 26.37$\pm$3.56 K and a minimum of 16.32$\pm$1.47 K with an offset of 10.06K. The average temperature is 19.25$\pm$0.15 K. Similarly, using WISE data, the temperature is found between a maximum of 353.72$\pm$18.54 K and a minimum of 307.24$\pm$4.69 K with an offset of 46.48K. The average temperature is 316.62$\pm$0.81 K. High value of offset temperature suggests that the cavity might be evolving with disruptions from background radiative sources. Approximately Gaussian distribution of the temperature in all the surveys implies that the region might be tending towards local thermodynamic equilibrium. The total mass of the structure is estimated to be around $0.03\pm1.5\times10^{-6}M_\odot$, $1.6\times10^{-3}\pm1.4\times10^{-5}$ $M_\odot$, and $10^{-7}\pm3\times10^{-10}$ $M_\odot$ using IRIS, AKARI, and WISE data respectively. The Jean's mass of the structure is calculated assuming the structure is a non-degenerate gas, which is estimated around $2001.93M_\odot$, $178.44M_\odot$, and $121.47M_\odot$ respectively using IRIS, AKARI, and WISE data. Since Jean's mass is much greater than the mass of the structure there seems no possibility of star formation within the region of interest. The color maps illustrate identical distribution for all wavelengths, however, no significant relation is observed between dust color temperature and dust mass.

Received: 25 August 2022; **Accepted**: 19 November 2022; **Published**: 31 December 2022

Keywords: White Dwarf; IRIS; AKARI; WISE; Dust color temperature

INTRODUCTION

During the lifetime of a star, depending on its total mass, much of the material born out may return to the ISM through stellar winds and explosive events like He-shell flash. The process of emissions into the ISM may be destructive; stellar winds result in erosion and fragmentation in supernovas thus generating the shock waves, or constructive via mantle accretion followed by coagulation in more dormant regions [1]. The subsequent generation of stars can thus be formed from these transferred materials [2]. In the left phase of the post-main sequence evolution in the HR diagram, these materials, a source of FIR

emissions, are found to be surrounding the WDs with a small fraction of dust formed in the circumstellar shells and cavities.

The radiation from ISM dust, confined within the molecular clouds, is the source of emissions from very cold objects: typically less than 140 K [3]. These dust structures obscure relatively nearby regions in visible and UV regions and re-radiate the absorbed radiation in the FIR region. This contributes a major part (30%) of the total luminosity of the galaxy. These FIR radiations preponderate over the gravitational energy of collapsing clouds, instigating star formations. Moreover, dust structures being responsible for the molecular dissociation and successively resulting H_2 molecule formation site, are crucial in studying the chemistry of ISM. Constituting most of the elements contributing to the cooling process, dust also controls the temperature of the ISM. On the other hand, it provides heat through electrons-photo-electrically ejected from the grains i.e. cold emission of electrons [4]. Such dust structures are pivotal in the study of interaction phenomena in the ISM.

In this work, we have studied the properties of an isolated dust structure nearby the white dwarf WD0011-399, searched through the Villanova catalog of spectroscopically identified white dwarfs, maintained by the department of astronomy and astrophysics, Villanova University, Pennsylvania [5]. The studied properties include flux density distribution, dust color temperature, dust mass, Jean's mass, spectral emissivity, and inclination angle along with background radiation sources.

SOURCES OF DATA

A series of methods were applied for locating an appropriate region of interest. Initially, the white dwarfs along with candidate white dwarfs were located using the published white dwarf catalogs and databases such as the white dwarf catalog of Villanova University [5], Montreal White Dwarf Database (MWDD) [6], and SIMBAD astronomical database (`https://simbad.u-strasbg.fr/simbad`). Furthermore, these databases were very useful in the verification of white dwarf candidates along with other astronomical bodies around them. Data is primarily obtained from SkyView virtual observatory (`https://skyview.gsfc.nasa.gov`) which generates images of any part of the sky at wavelengths in all regimes from Radio to Gamma-Ray. Data from all the surveys are obtained in the form of a Flexible Image Transport System (FITS) image which embodies the data regarding flux density, coordinates, and pixel location which were extracted using Aladin v10.0 [7]. Moreover, for distance estimation parallax data from Gaia [8] is taken around the structure and the SIMBAD database is of assistance in locating the background sources.

METHOD

Dust Color Temperature

The dust color temperatures for IRIS, AKARI, and WISE surveys were calculated based on Wood et al. [9] and later improved by Dupac et al. [10] and Schnee et al. [11]. The final expression for dust color temperature in the case of IRIS 60 and 100 μm data is,

$$T_d = \frac{-96}{ln\{R \times 0.6^{(3+\beta)}\}} \tag{1}$$

where R is the ratio of the flux densities at 60 μm and 100 μ and β is the spectral emissivity index ranging from 0 to 2 depending on the dust grain properties.

$$\beta = \frac{1}{\delta + \omega T_d} \tag{2}$$

where parameters δ and ω depend on the dust grain properties like composition, size, compactness, and so on and have values $\delta = 0.40 \pm 0.02$ and $\omega = 0.0079 \pm 0.0005 K^{-1}$ [10].

Similarly for AKARI data at 90 and 140 μm,

$$T_d = \frac{-57}{ln\{R \times 0.6^{(3+\beta)}\}} \tag{3}$$

Following the same procedures, for WISE data at 12 and 22 μm equation (1) can be modified as,

$$T_d = \frac{-545}{ln\{R \times 0.6^{(3+\beta)}\}} \tag{4}$$

Dust Mass and Jean's Mass Estimation

Dust mass depends on the physical as well as chemical properties of the dust grains, dust color temperature(T_d), and the distance(D) to the structure [12].

$$M_d = \frac{4a\rho}{3Q_\nu}\left[\frac{F_\nu D^2}{B(\nu, T_d)}\right] \tag{5}$$

where a = weighted grain size (0.1 μm)
ρ = grain density (3000 kgm^3)
Q_ν = grain emissivity (0.001 for 100 μm and 0.0046 for 60 μm)
F_ν = total flux density of the region

$B(\nu, T_d)$ is Planck's function for black-body radiation at temperature T_d and frequency ν,

$$B(\nu, T_d) = \frac{2h\nu^3}{c^2}\left[\frac{1}{e^{\frac{h\nu}{k_B T_d}} - 1}\right] \tag{6}$$

where h = Planck's constant
c = speed of light in vacuum
k_B = Boltzmann's constant.

Implementing the substitutions by Young et al. [13], equation (5) is reduced to,

$$M_d = 0.4\left[\frac{F_\lambda D^2}{B(\lambda, T_d)}\right] \tag{7}$$

For a dust structure to be stable, it must be in hydrostatic equilibrium. If the internal pressure of the gas is greater than the gravitational force then the mass will collapse and instability occurs which is known as Jeans instability. It depends on the average temperature (T_d), density (ρ), and size (R) of the cloud [2]. Once the size and the temperature of the region are known, assuming the molecular cloud is extremely cold the equation of state for a non-degenerate case can be applied to determine the density can be calculated as,

$$\rho = \left(\frac{3}{4\pi}\right)^{\frac{2}{3}}\left[\frac{k_B T_d}{m_H G R^2}\right] \tag{8}$$

where m_H = mass of hydrogen
G = universal gravitational constant
R = radius of the molecular cloud considering its spherical shape [14].
Jean's mass can thus be calculated as,

$$M_J = \frac{K}{\sqrt{\rho}}\left(\frac{k_B T_d}{\mu G}\right)^{\frac{3}{2}} \tag{9}$$

where K is the proportionality constant which depends on the nature of perturbation. The perturbation depends on the speed of acoustic waves and the adiabatic index [2]. For slow varying perturbation,

$$K = \frac{4}{3}\pi^{\frac{5}{2}} \tag{10}$$

Inclination Angle

The inclination angle (i) is the angle between the line of sight and the normal vector to the plane of the structure. This can be estimated by using the formula given by Holmberg et al. [15],

$$cos^2 i = \frac{(\frac{b}{a})^2 - q*^2}{1 - q*^2} \tag{11}$$

where $\frac{b}{a}$ is the ratio of minor to major diameter and $q*$ is the intrinsic flatness of the structure. The intrinsic flatness is closely related to nebula morphology. It depends on the amount of molecular hydrogen and dust. The range of the intrinsic flatness of the cloud extends from 0.13 to 0.33. For convenience, the average value of 0.23 is considered for molecular cloud-type structure. [16]

RESULT AND DISCUSSION

Structure

The structural visualization of the dust structure from the available FITS image is done in Aladin v10.0. The pixel color values were adjusted for clear visualization and different levels of isocontours were drawn around the cavity distinguishing the cavity region from the rest parts of the image and thus aiding in the distinction of pixels with the maximum flux density. The pixel location of maximum flux density acts as a point of intersection of the major and minor axes of the region of interest. In IRIS (100 μm), AKARI (140 μm), and WISE (22 μm) FITS images, the maximum flux densities were 47.45, 129.94 and 166.33 MJysr^{-1} respectively. On drawing the longest and shortest axes passing through the maximum flux density pixel and joining the opposite ends of the contour, the obtained major axis and minor axis in the IRIS FITS image are 26.08' and 10.17' respectively thus the angular dimension of the region of interest is 26.08'×10.17'. Following a similar procedure in AKARI FITS image, the angular dimension is estimated to be 10.47'×3.48'. Similarly in the WISE FITS image, the angular dimension is 4.45'×1.89'.

The angular dimension is converted to linear dimension by using the formula,

$$l = d \times \theta \tag{12}$$

where angular dimension θ is in radian.

The distance (d) is estimated from Gaia data using the parallax method as 979.49 pc. Thus the linear dimension of the region of interest is approximated to be 7.43 pc×2.90 pc, 2.99 pc×0.99 pc, and 1.26 pc×0.53 pc in IRIS, AKARI, and WISE respectively. The difference in dimensions of the isolated structure in different surveys is due to non-identical FITS image resolutions. The resolution of the IRIS FITS image is the highest and that of WISE is the lowest. The direct proportionality between image resolution and structure thus resulted in the largest dimension for the IRIS image and the smallest for the WISE image.

TABLE I. General Description of FITS Image Data and Isolated Structures in all Surveys

Surveys	Image Size	Angular Size (arc min)	Linear Size (parsec)
WISE (22μm)	0.1^o	4.45'×1.89′	1.26×0.53
IRIS (100μm)	0.5^o	26.08'×10.17′	7.43×2.90
AKARI (140μm)	0.18^o	10.47'×3.48′	2.99×0.99

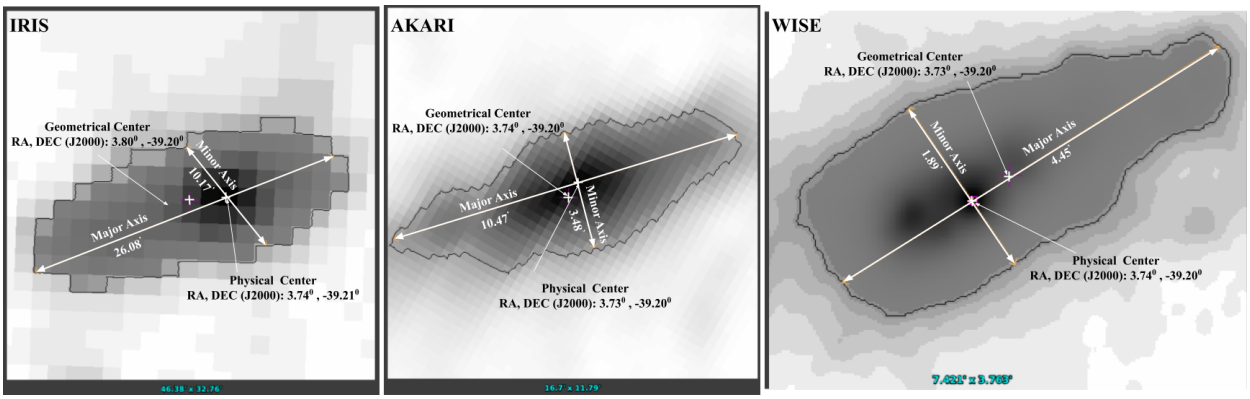

FIGURE 1. Structure of Region of Interest in IRIS, AKARI, and WISE FITS Images; Respective Image Resolutions: ($46.38^{'} \times 32.76^{'}$), ($16.70^{'} \times 11.79^{'}$), and ($7.42^{'} \times 3.76^{'}$). The Intensity of Pixels Corresponds the Flux Density Values.

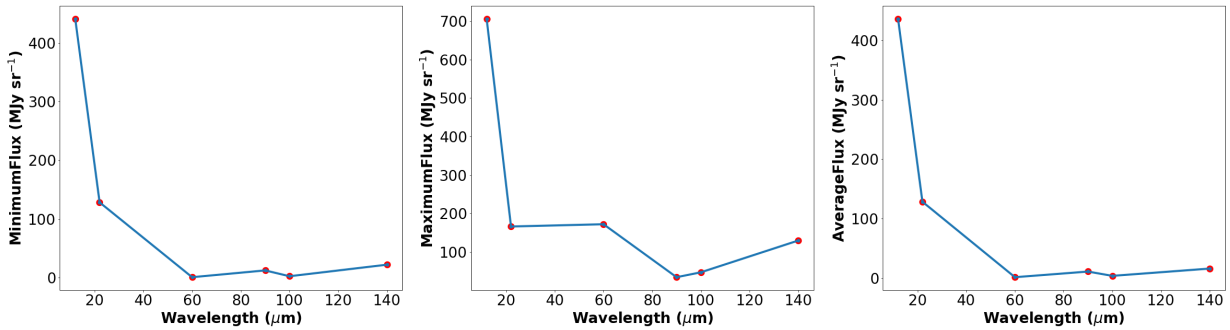

FIGURE 2. Scatter Plot of Flux Densities against Wavelengths Showing Uniformity Across the Surveys

Flux Density Distribution

The flux density distribution was visualized in IRIS, AKARI, and WISE data using contour plots. These relative flux densities were later used for the calculation of dust color temperature.

On plotting the maximum, minimum, and average flux densities each separately against their respective wavelengths, the scatter plot, **FIGURE 2** obtained is of similar nature. This shows a uniform flux distribution across the surveys.

TABLE II. Flux Densities for Different Wavelengths

Wavelength (μm)	Flux density (MJysr^{-1})		
	Minimum	Maximum	Average
12	440.62	705.20	435.51
22	128.22	166.33	128.54
60	0.738	34.66	1.79
90	12.31	172.22	11.27
100	2.39	47.44	4.05
140	22.04	129.94	16.29

Flux Density Relation

Flux densities at two different wavelengths for each survey were plotted against each other as depicted in **FIGURE 3**, to determine the relationship between them. In IRIS data, the relationship between relative flux densities at 60 and 100 μm is found to be linear with a correlation coefficient of 0.95. In AKARI data, the relationship between relative flux densities at 90 and 140 μm is parabolic with a correlation coefficient of 0.88. Similarly in WISE data, the relation between relative flux densities at 12 and 22 μm is obtained to be linear with a correlation coefficient of 0.96.

In general, the correlation between relative flux densities at two different wavelengths of the same survey is very high and positive which is as expected.

Dust Color Temperature

The dust color temperature for IRIS, AKARI, and WISE data was calculated as given by equations (1), (3), and (4) respectively. Assuming the dust as crystalline dielectric

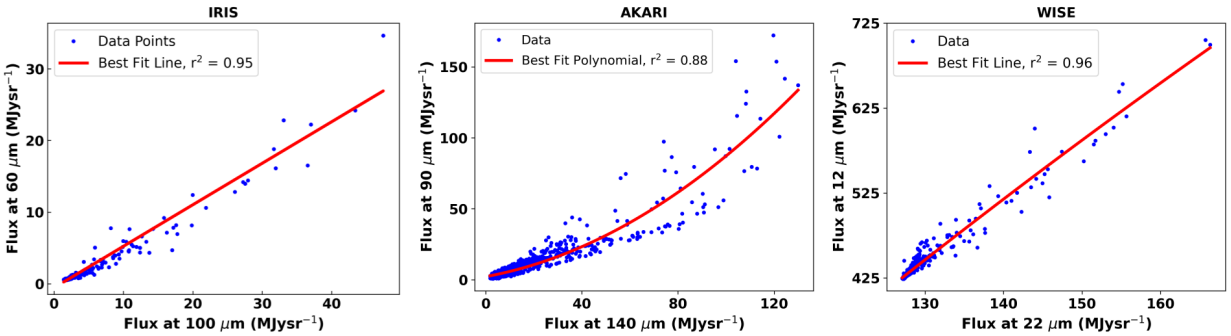

FIGURE 3. Flux Density Relationship Between Different Wavelengths of the Same Survey

β=2 was chosen. With the IRIS data, the temperature of the region of interest is found between a minimum value of 22.59±2.32 K to a maximum value of 36.82±4.30 K with an offset of 14.23 K and an average temperature of 28.22±0.18 K. Using AKARI data, the temperature is found between a minimum of 16.31±1.47 K and a maximum of 26.37±3.56 K with an offset of 10.06 K and an average temperature of 19.25±0.15 K. Similarly in WISE data, the temperature is found between a minimum of 307.24±4.69 K and a maximum of 353.72±18.54 K with an offset of 46.48 K and an average temperature of 316.62±0.81 K.

TABLE III. Temperature Distribution for Different Wavelengths

Surveys	**Temperature (K)**			
	Minimum	**Maximum**	**Offset**	**Average**
IRIS	22.59 ± 2.32	36.82 ± 4.30	14.23	28.22 ± 0.18
AKARI	16.31 ± 1.47	26.37 ± 3.56	10.06	19.25 ± 0.15
WISE	307.24 ± 4.69	353.72 ± 18.54	46.48	316.62 ± 0.81

Since the temperature of the dust structure is low (below 30K) in IRIS and AKARI data, the structure under study is mostly composed of cool dust grains [17]. Moreover, the high value of offset temperature suggests that the structure might be evolving with disruptions from background radiative sources. According to Wien's displacement law (for lower wavelengths and temperatures), the wavelength of black-body radiation (λ) is inversely proportional to the temperature (T), given by

$$\lambda = \frac{b}{T} \tag{13}$$

where b is Wien's displacement constant $\approx 2898\ \mu$mK.

From **TABLE II** it is conspicuous that the temperature data for all surveys are in correspondence with Wien's displacement law. Moreover, the distribution of the temperature in all the surveys is found to be approximately Gaussian in nature as shown in **FIGURE 4**. Low temperatures and approximately Gaussian distributions of temperature suggest that the structure is tending towards thermodynamic equilibrium.

Dust Mass and Jean's Mass

The dust mass of the isolated region (M_d) is calculated as given by equation (7) under the stated premises. The distance calculated from Gaia data using the parallax method is used for mass estimation. The mass of gas in the structure (M_G) is estimated considering the mass of the gas in ISM is about 200 times that of the dust [12]. The dust mass of the isolated region is estimated to be $0.03\pm1.5\times10^{-6}M_\odot$, $1.6\times10^{-3}\pm1.4\times10^{-5}M_\odot$, and $10^{-7}\pm3\times10^{-10}M_\odot$ respectively for IRIS, AKARI, and WISE data. Similarly, the gas mass is calculated to be $5.15\pm3\times10^{-4}M_\odot$, $0.31\pm2.8\times10^{-3}M_\odot$, and 9.75×10^{-5} $\pm6\times10^{-8}M_\odot$ respectively in IRIS, AKARI, and WISE surveys.

The parallax data from Gaia is used to roughly determine the 3D information of the structure and considering the clouds to be cold; derived from wavelengths, Jean's mass of the isolated dust structure, $(M_J)_D$ is estimated by applying a simple non-degenerate model. The Jean's masses of the structure are estimated around $178.44M_\odot$, $121.47M_\odot$, and $2001.93M_\odot$ using IRIS, AKARI, and WISE data respectively. Since Jean's masses for all the surveys are far greater than the masses of the structure, theoretically the gravity of the structure is not dominant enough for gravitational collapse. Thus there seems no possibility of star formation within the region of interest.

Spectral Emissivity

On plotting spectral emissivity against average temperature in IRIS and AKARI data, the relationship is found to be parabolic with a correlation coefficient = 1. However,

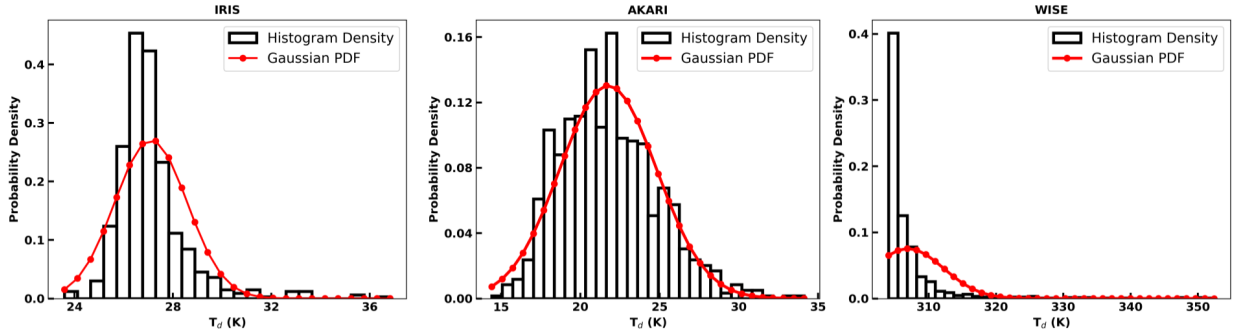

FIGURE 4. Gaussian Distribution of Temperature in IRIS, AKARI and WISE Data. The IRIS and AKARI Data are Gaussian Distributed while the WISE Data is Deviated from Gaussian: More Specifically Hyperbolic

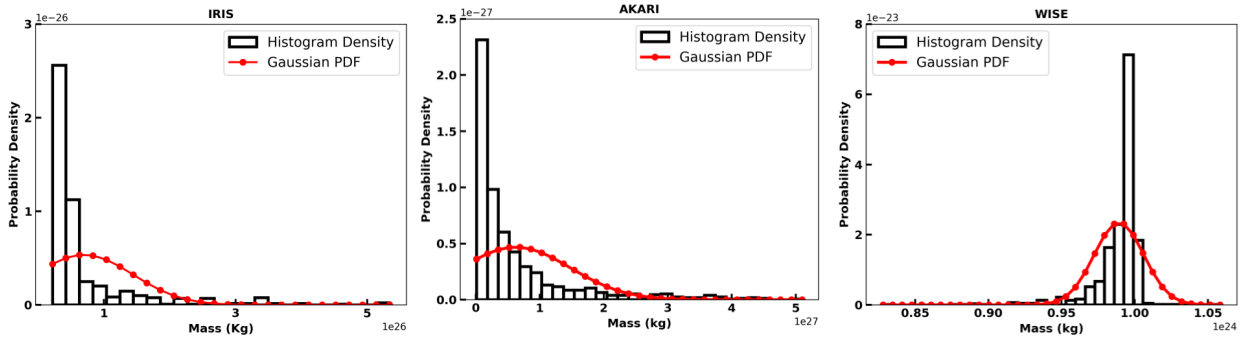

FIGURE 5. Gaussian Distribution of Mass in IRIS, AKARI and WISE Data. The IRIS and AKARI Data are Deviated from Gaussian Distribution (Hyperbolic) while the WISE Data is Gaussian Distributed.

TABLE IV. Mass of Dust, Gas and Jean's Mass for Different Surveys

Surveys	**Mass ($M_\odot$)**		
	$\mathbf{M_d}$	$\mathbf{M_G}$	$\mathbf{(M_J)_D}$
WISE	$10^{-7}\pm3\times10^{-10}$	$9.75\times10^{-5}\pm6\times10^{-8}$	2001.93
IRIS	$0.03\pm1.5\times10^{-6}$	$5.15\pm3\times10^{-4}$	178.44
AKARI	$1.6\times10^{-3}\pm1.4\times10^{-5}$	$0.31\pm2.8\times10^{-3}$	121.47

in WISE data, there exists 7th-degree polynomial relation as shown in the **FIGURE 6**.

Inclination Angle

The estimated major axis (a) and minor axis (b) from Aladin v10.0 are used to calculate the inclination angle according to equation (11), assuming an average intrinsic flatness of the nebula to be 0.23 [16]. The inclination angles are approximately the same for all the surveys which are as expected because it represents the inclination of the structure from the galactic plane which should be equivalent for all the surveys. The inclination angle is neither close to zero (face-on) nor close to 90^o (edge-on) [18]. Face-on implies a spherical structure (parallel to the galactic plane) and edge-on implies an ellipsoidal structure (perpendicular to the galactic plane). Moreover, the ratio of the minor axis to the major axis is less than 0.5 which implies the dust structure is neither spherical nor ellipsoidal, however, somewhat deviated towards an ellipsoidal structure.

TABLE V. Inclination Angle of the Dust Structure in Different Surveys

Surveys	**b/a Ratio**	**Inclination Angle (degrees)**
IRIS (100μm)	0.39	71.12
AKARI (140μm)	0.33	75.73
WISE (22μm)	0.42	68.48

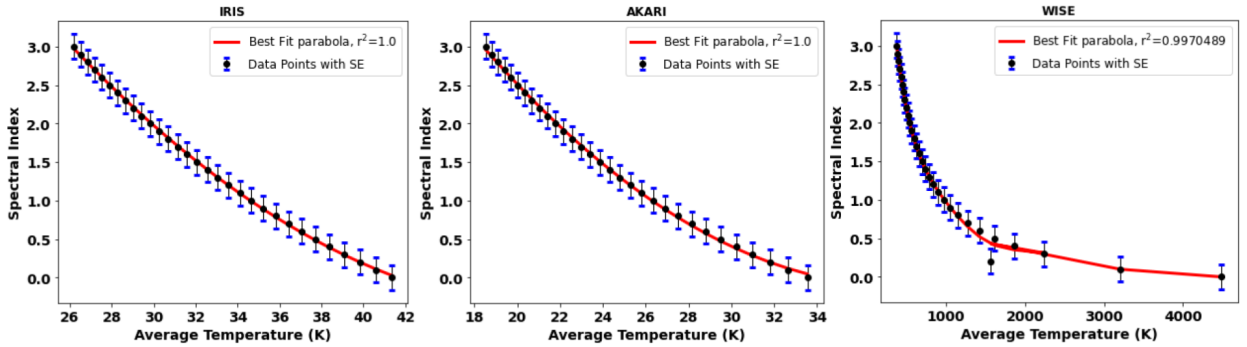

FIGURE 6. Emissivity and Average Temperature Relation in IRIS, AKARI and WISE Data. Each Data Point Signifies the Average Temperature Corresponding to Indices of Spectral Emissivity.

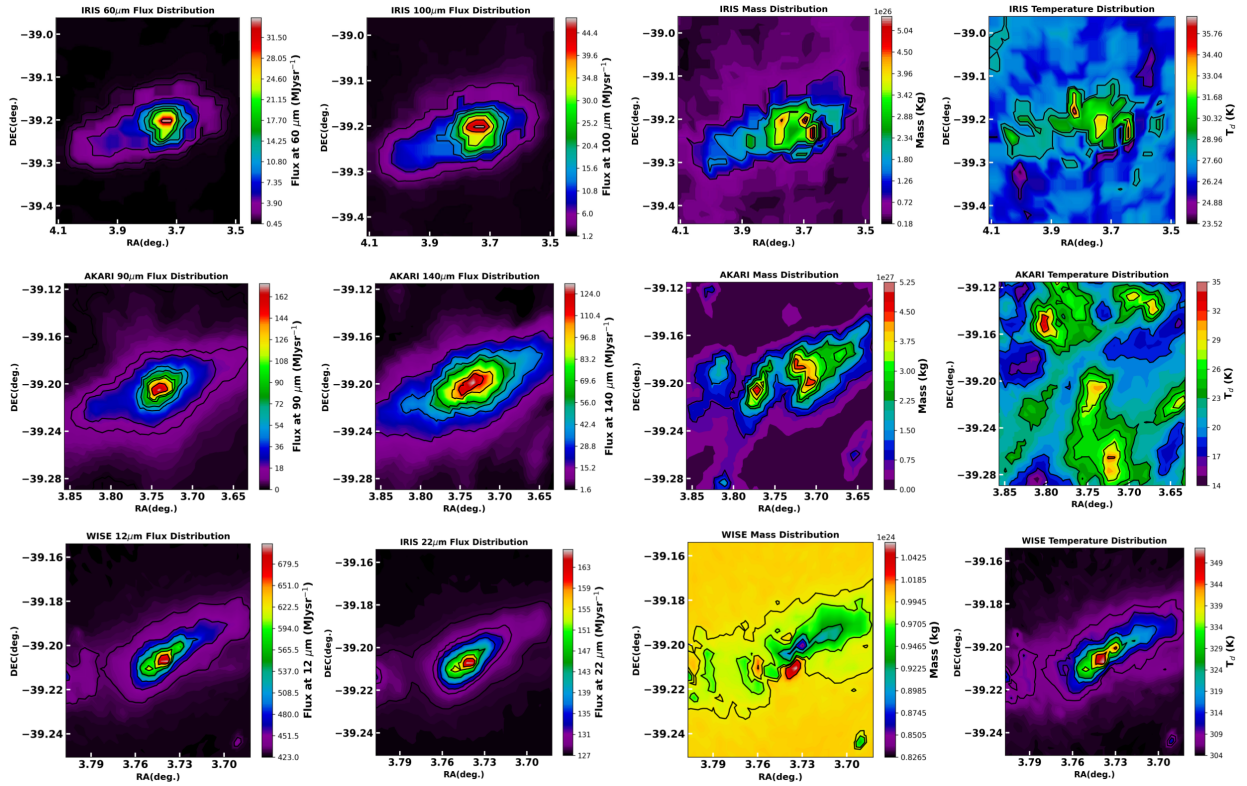

FIGURE 7. Isocontour Plots of Flux Densities, Mass and Temperature Distributions in IRIS, AKARI and WISE Data

Isocontour Map

Iso-contour maps on **FIGURE 7** show a variation in the distribution of IR flux density, temperature, and mass on IRIS, AKARI, and WISE data. From the study of the flux density distributions, it is found that the intensity of flux density gradually increases towards the center of the structure. Since the isolated structure is nebular, higher flux density near the core is expected. Analyzing all the surveys, the flux density distribution is found to be proportional to the operating wavelength. Moreover, the flux density distribution smoothly varies between various contour levels commensurate with the resolution of the survey telescopes.

From the side-by-side comparison of flux density and mass distributions, a direct relation between flux density and mass is observed. In all the surveys, the regions with higher flux density also have higher mass. As the structure is nebular, the region with high flux density implies the accumulation of a larger amount of dust in

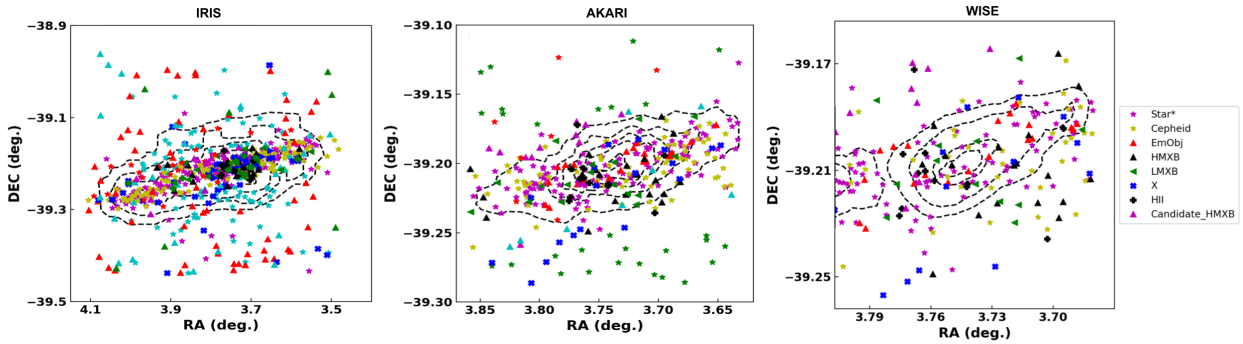

FIGURE 8. Background Sources Obtained From SIMBAD Data Against the Isocontours of Mass Distributions

that region thus making it massive. The relationship visualized from the contour plot is in agreement with the explanation. However, in AKARI data, lesser mass distribution is found in some regions with high flux density and in WISE data, regions with low flux density are observed to be comparatively of low mass. This might be due to the very low operating wavelength of WISE along with the presence of a lot of background sources nearby the structure.

On the other hand, the comparison between temperature and mass distribution for different surveys led to the inference that there exists no direct correspondence between temperature and mass in IRIS and AKARI data. While in WISE data, the region with high-temperature distribution is found to have higher mass distribution and those with low-temperature distribution are found to have low mass distribution.

Background Sources

Background astronomical objects around the dust structure are obtained from SIMBAD astronomical database. Within the radius of 20' around the coordinates RA (ICRS): 3.79^o and Dec. (ICRS): -39.20^o, there are 809 astronomical objects among which stars are found dominant.

The presence of a such large number of astronomical objects around the structure has a major influence on the properties of the structure. The deviation of the distribution of mass as well as temperature from Gaussian distribution can be interpreted as the influence of these background astronomical objects. From the analysis of **FIGURE 8** it can be interpreted that within the regions of higher mass, astronomical objects like stars, cepheids, and emission objects are dominant. Since stars are continually radiating energy, cepheids are radially pulsating causing variation in their diameter and temperature, and emission objects, as the name suggests emit energy, the distribution of mass as well as temperature is highly influenced by their presence in the background.

CONCLUSION

Various properties such as infrared flux density distribution and relation, dust color temperature, dust mass, Jean's mass, distance, inclination angle, and spectral emissivity of the dust structure nearby the white dwarf WD0011-399, located at RA(J2000): $00^h\ 13^m\ 47.48^s$, Dec.(J2000): -39° 37′ 24.28″, were studied. The following are the major conclusions of this research work:

- The size of the dust structure is estimated to be $26.08' \times 10.17'$ (7.43 pc×2.90 pc), $10.47' \times 3.48'$ (2.99 pc×0.99 pc) and $4.45' \times 1.89'$ (1.26 pc×0.53 pc) in IRIS, AKARI, and WISE data respectively.
- For the same survey, the flux density is directly proportional to the wavelength in case of longer wavelengths, i.e., 60−140 μm. However, the relation is just the opposite in the case of shorter wavelength i.e. 12−22 μm.
- The average temperature of the isolated region is estimated to be 28.22±0.18 K in IRIS, 19.25±0.15 K in AKARI, and 316.62±0.81 K in WISE data. The relation between wavelength and temperature is in accordance with Wien's displacement law.
- The study of the contour map shows there is no direct relation between the distribution of mass and temperature in IRIS and AKARI data. However, there exists a direct relation between them in WISE data.
- The central part of the isolated region has the highest temperature as well as mass than the outer regions, representing the central region is thermally active and compact while the outer region is thermally stable.

- The distance of the dust structure is estimated to be 979.49 pc.
- The study of background sources in the SIMBAD database shows a large number of background objects near the structure which might be responsible for the contribution of dust temperature and dust mass within the dust structure.
- The temperature and mass distribution is close to the Gaussian distribution which might indicate the asymmetric distribution of ISM sources, such as; dense core, part of the cloud, radio (sub-mm) source, and the like, which are observed in the SIMBAD database.
- Inclination angle is estimated to be 71.12°, 75.73° and 68.48° with minor to major axis ratios of 0.39, 0.33 and 0.42 in IRIS, AKARI, and WISE data respectively. This shows that the isolated region within the dust structure is neither face-on nor edge-on, however, the structure is slightly deviated from its spherical shape.

ACKNOWLEDGMENTS

We would like to express our profound gratitude to the Department of Physics, Tri-Chandra Multiple Campus, Tribhuvan University, Nepal for providing the academic environment to conduct this work and the University Grants Commission (UGC), Research Division, Sanothimi, Bhaktapur, Nepal for sponsoring this research work (Award No.: SRDIG–77/78–ST–5). We are also grateful to the SkyView virtual observatory, IRIS, AKARI, WISE, white dwarf catalog of Villanova university, SIMBAD, and Gaia archive for the sources of data.

EDITOR'S NOTE

This manuscript was submitted to the Association of Nepali Physicists in America (ANPA) Conference 2022 for publication in the special issue of the Journal of Nepal Physical Society.

REFERENCES

1. A. G. Tielens, *The physics and chemistry of the interstellar medium* (Cambridge University Press, 2005).
2. B. Carroll and D. Ostlie, *An Introduction to Modern Astrophysics*, 2nd ed. (Pearson Education Limited, 2014) pp. 456–458.
3. W. Kundt, *Astrophysics: a new approach* (Springer Science & Business Media, 2004).
4. E. Böhm-Vitense, *Introduction to Stellar Astrophysics: Volume 3*, Vol. 3 (Cambridge University Press, 1992).
5. G. P. McCook and E. M. Sion, "A catalog of spectroscopically identified white dwarfs," The Astrophysical Journal Supplement Series **121**, 1 (1999).
6. P. Dufour, S. Blouin, S. Coutu, M. Fortin-Archambault, C. Thibeault, P. Bergeron, and G. Fontaine, "The montreal white dwarf database: a tool for the community," arXiv preprint arXiv:1610.00986 (2016).
7. F. Bonnarel, P. Fernique, O. Bienaymé, D. Egret, F. Genova, M. Louys, F. Ochsenbein, M. Wenger, and J. G. Bartlett, "The aladin interactive sky atlas-a reference tool for identification of astronomical sources," Astronomy and Astrophysics Supplement Series **143**, 33–40 (2000).
8. A. G. Brown, A. Vallenari, T. Prusti, J. De Bruijne, C. Babusiaux, M. Biermann, O. Creevey, D. Evans, L. Eyer, A. Hutton, *et al.*, "Gaia early data release 3-summary of the contents and survey properties," Astronomy & Astrophysics **649**, A1 (2021).
9. D. O. Wood, D. A. Daugherty, and P. C. Myers, "Iras images of nearby dark clouds," Astrophysics Journal and Supplement Series **95**, 457–501 (1994).
10. X. Dupac, J.-P. Bernard, N. Boudet, M. Giard, J.-M. Lamarre, C. Mény, F. Pajot, I. Ristorcelli, G. Serra, B. Stepnik, *et al.*, "Inverse temperature dependence of the dust submillimeter spectral index," Astronomy & Astrophysics **404**, L11–L15 (2003).
11. S. L. Schnee, N. A. Ridge, A. A. Goodman, and J. G. Li, "A complete look at the use of iras emission maps to estimate extinction and dust temperature," The Astrophysical Journal **634**, 442 (2005).
12. R. H. Hildebrand, "The determination of cloud masses and dust characteristics from submillimetre thermal emission," Quarterly Journal of the Royal Astronomical Society **24**, 267 (1983).
13. K. Young, T. Phillips, and G. Knapp, "Circumstellar shells resolved in iras survey data. ii-analysis," The Astrophysical Journal **409**, 725–738 (1993).
14. H. Karttunen, P. Kröger, H. Oja, M. Poutanen, and K. J. Donner, *Fundamental astronomy*, Vol. 4 (Springer, 2007).
15. E. Holmberg, "Investigations of the systematic errors in the apparent diameters of the nebulae," **117** (1946).
16. M. P. Haynes and R. Giovanelli, "Neutral hydrogen in isolated galaxies. iv-results for the arecibo sample," The Astronomical Journal **89**, 758–800 (1984).
17. E. Xilouris, F. Tabatabaei, M. Boquien, C. Kramer, C. Buchbender, F. Bertoldi, S. Anderl, J. Braine, S. Verley, M. Relaño, *et al.*, "Cool and warm dust emission from m 33 (herm33es)," Astronomy & Astrophysics **543**, A74 (2012).
18. A. Jha and B. Aryal, "Dust color temperature distribution of two fir cavities at iris and akari maps," Journal of Astrophysics and Astronomy **39**, 5–6 (2018).